frontiers | Frontiers in Earth Science

TYPE Original Research
PUBLISHED 19 December 2023
DOI 10.3389/feart.2023.1306460

OPEN ACCESS

EDITED BY
Simona Ferrando,
University of Turin, Italy

REVIEWED BY
Rosario Esposito,
University of Milano-Bicocca, Italy
Tong Hou,
China University of Geosciences, China

*CORRESPONDENCE
Olga A. Andreeva,
oandreeva@igem.ru

RECEIVED 03 October 2023
ACCEPTED 06 December 2023
PUBLISHED 19 December 2023

CITATION
Andreeva OA, Dubinina E, Andreeva IA, Yarmolyuk VV, Bychkov A, Borisova A, Ji J, Zhou X, Kovalchuk EV, Borisovsky SY and Averin AA (2023), Mechanism of carbonate assimilation by intraplate basaltic magma and liquid immiscibility: example of Wangtian'e volcano (Changbaishan volcanic area, NE China). *Front. Earth Sci.* 11:1306460.
doi: 10.3389/feart.2023.1306460

Mechanism of carbonate assimilation by intraplate basaltic magma and liquid immiscibility: example of Wangtian'e volcano (Changbaishan volcanic area, NE China)

Olga A. Andreeva[1]*, Elena Dubinina[1], Irina A. Andreeva[1], Vladimir V. Yarmolyuk[1], Andrey Bychkov[2], Anastassia Borisova[3], Jianqing Ji[4], Xin Zhou[4], Elena V. Kovalchuk[1], Sergey Y. Borisovsky[1] and Alexey A. Averin[5]

[1]Institute of Geology of Ore Deposits, Petrography, Mineralogy and Geochemistry, Russian Academy of Sciences, Moscow, Russia, [2]Department of Geology, Lomonosov Moscow State University, Moscow, Russia, [3]Géosciences Environnement Toulouse, Observatoire Midi-Pyrénées, Université Toulouse III/CNRS/IRD/CNES, Toulouse, France, [4]School of Earth and Space Sciences, Peking University, Beijing, China, [5]Frumkin Institute of Physical Chemistry and Electrochemistry, Russian Academy of Sciences, Moscow, Russia

The balance of CO_2 during abundant basaltic magma production is an important factor of volcanic hazards and climate. In particular, this can be explored based on CO_2-rich mantle-derived magmas or carbonate assimilation by basaltic melts. To reconstruct the origin of Fe-rich carbonates hosted by Cenozoic basalts from Wangtian'e volcano (northeast China), we studied elemental compositions of melt, crystalline and fluid inclusions in magmatic minerals as well as the oxygen and carbon isotope compositions of the plagioclase and carbonates from basalts. The crystallization of basaltic magmas occurred in shallow chamber (~4 km) at temperatures of 1,180°C–1,200°C and a pressure of 0.1 ± 0.01 GPa. Stable Fe-rich carbonates occur in the Wangtian'e tholeiite basalts as groundmass minerals, crystalline inclusions in plagioclase and globules in melt inclusions, which suggests that they crystallized from a ferrocarbonate melt. The values of $\delta^{18}O$ and $\delta^{13}C$ in the minerals analyzed by laser fluorination method are in line with the sedimentary source of Fe-rich carbonates, indicating assimilation and partial decomposition of carbonate phases. The parent ferrocarbonate melt could be produced during interactions between the basaltic magma and the crustal marbles. The phase diagram and thermodynamic calculations show that the ferrocarbonate melt is stable at a temperature of 1,200°C and a pressure of 0.1 GPa. Our thermodynamic calculations show that carbonate melt containing 73 wt% $FeCO_3$, 24 wt% $MgCO_3$ and 3 wt% $CaCO_3$ is in thermodynamic equilibrium with silicate melt in agreement with our natural observations. The proposed mechanism is crustal carbonate sediment assimilation by the intraplate basaltic magma resulting in the melt immiscibility, production of the ferrocarbonate melt and the following Fe-rich carbonate mineral crystallization during magma residence and cooling.

KEYWORDS

intraplate volcanism, melt inclusions, fluid inclusions, silicate liquid immiscibility, silicate-carbonate liquid immiscibility, ferrocarbonates

1 Introduction

Up to date, carbon source and mechanisms of the carbonate formation in basaltic magma remain unclear, whereas the balance of CO_2 during basaltic magmas production is an important factor of volcanic hazards and climate (Martini, 1997; Tobin et al., 2017). For example, origin of ferrocarbonates (or Fe-rich carbonates) genetically associated with basaltic lavas is an unresolved problem (Viladkar and Schidlowski, 2000; Xue and Zhu, 2007; Viladkar, 2018; Randive and Meshram, 2020). Ferrocarbonatite veins and lenses related to flood basalts have been described in the Siberian and Deccan traps (Randive and Meshram, 2020). In addition, siderite of magmatic origin is found in the Jurassic olivine basalts of the Karamay province in northwest China (Xue and Zhu, 2007) and metastable calcite and carbonate melt is reported by Borisova and Bohrson (2023) for Merapi volcano (Indonesia) as well as Na-K-Ca carbonate-chloride melt recorded in melt inclusions at Mount Vesuvius studied by Fulignati et al. (2001) and Klebesz et al. (2015). Nevertheless, such studies are extremely scarce and the mechanism of the carbonate assimilation and the following melt immiscibility in the contest of basaltic magma remains unknown. The present study is of particular interest since it focuses on the origin of Fe-rich carbonates in the Cenozoic intraplate tholeiitic basalts of Wangtian'e volcano in the Changbaishan area of northeast China.

Two hypotheses can be considered. 1) The ferrocarbonates can also be formed during the decarbonation of sedimentary carbonates trapped by the basaltic magma or by interaction between basaltic melts and sedimentary carbonates of the continental crust. 2) The CO_2 excess in basaltic magmas can be produced by partial melting of metasomatized mantle. Numerous experimental works devoted to pure carbonate solubility in mafic melts demonstrate an important role of carbonate material on the magma liquidus phase stability field (Freda et al., 2008; Iacono-Marziano et al., 2008; 2009; Mollo et al., 2010). Additionally, Deegan et al. (2010), Jolis et al. (2013) and Blythe et al. (2015) experimentally studied interaction of carbonate materials with mafic and alkaline melts at conditions corresponding to the deep crust (5 kbar) resulting in chemical reactions between carbonates and silicates with CO_2 exsolving. Nevertheless, the mechanisms of ferrocarbonate melt formation in the shallow mafic magma chambers (up to 5 km) remain unclear. This paper reports results of petrological and geochemical studies on the Wangtian'e basalts, as well as carbon and oxygen isotope compositions, including the analyses of natural melt inclusions trapped by silicate minerals and thermodynamic calculations based on these natural data. Using these results, we propose a quantitative model for the formation of ferrocarbonates in the tholeiitic basalts of Wangtian'e volcano.

2 Geological setting of Wangtian'e volcano and timescale of its formation

The Changbaishan volcanic field (Figure 1) is spatially constrained to the northern margin of the Archean–Proterozoic Sino–Korean craton at the Chinese–North Korean border, at the intersection of the northeast-trending Tanlu rift system and the northwest-trending Paektusan faults (Andreeva et al., 2014; Andreeva et al., 2020). Two large stratovolcanoes are located within this volcanic field: Changbaishan and Wangtian'e. In contrast to the strongly differentiated alkaline series of Changbaishan (Fan et al., 1999; Andreeva et al., 2014; Andreeva et al., 2018; Andreeva et al., 2019), the lavas of Wangtian'e belong to the tholeiite series and show only slight variations in composition from basalts to basaltic andesites (Andreeva et al., 2022). The thick shield platform and cone of Wangtian'e volcano are composed of tholeiitic basalts. Silicic rocks form trachyte necks and a rhyolite extrusive dome (Fan et al., 1999; Andreeva et al., 2020; Andreeva et al., 2022).

The results of K-Ar age dating (Andreeva et al., 2022) indicate that the Wangtian'e volcano was formed within a short geological period of time between 3.8 and 2.7 Ma. The evolution of the volcano comprises three main stages: 1) Changbai period with fissure eruptions of basaltic lavas formed a shield volcano, 2) Wangtian'e period with growth of the basaltic cone, and 3) the Hongtoushan period, marked by the formation of necks and an extrusive dome of trachyte–alkaline rhyolite composition. We examined the northern, southern, and eastern slopes of the cone and the shield volcano and collected samples of all their major rock types. Below, we discuss the results of our geochemical studies of tholeiitic basalts from the southeastern section of the shield volcano (Figure 1).

3 Geochemical characteristics of tholeiitic basalts

The volcanic rocks from the southeastern section of the Wangtian'e shield volcano correspond to basalts with SiO_2 contents of 48.7–50.1 wt%., showing high Fe_2O_{3tot} (9.6–13.5 wt%) but low MgO (2.4–3.7 wt%). The basalts are also enriched in titanium (TiO_2 = 2.4–3.5 wt%) and phosphorus (P_2O_5 up to 1.2 wt%). The total alkali contents of the basalts vary from 4.3 to 5.2 wt% (Table 1). The AFM diagram (Figure 2) shows that the compositions of the shield basalts plot above the Irwin-Baragar line (Irwine and Baragar, 1971) and belong to tholeiitic series.

The basalts were collected from the bottom to the top along the southeastern section of the shield volcano. They all have similar petrographic features and chemical compositions (Table 1). Basalts are represented by massive dark gray porphyritic rocks with large

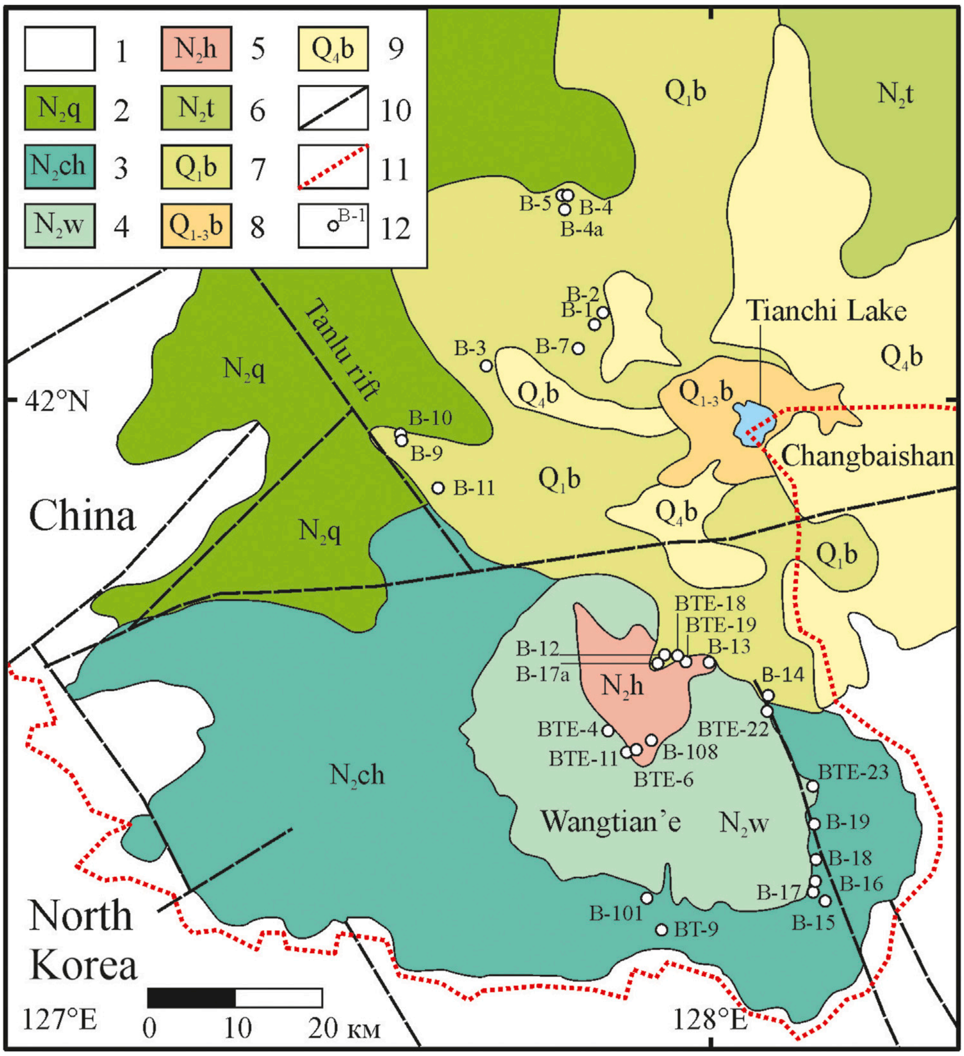

FIGURE 1
Geological sketch map of the Wangtian'e and Changbaishan volcanoes in the Changbaishan Mountains [modified after Andreeva et al. (2022)]. (1) host rocks; (2) flood basalts of the Changbaishan volcanic field, Quanyang period (4.50–4.00 Ma); (3) tholeiitic basalts of the Wangtian'e shield volcano, Changbai period (3.82–2.83 Ma); (4) tholeiitic basalts of the Wangtian'e volcano, Wangtian'e period (2.76–2.67 Ma); (5) dome and necks of Wangtian'e volcano, Hongtoushan period (2.76–2.69 Ma); (6) alkaline basalts of Changbaishan shield volcano, Toudao period (2.77–1.99 Ma); (7) alkaline basalts of Changbaishan shield volcano, Baishan period (1.64–1.11 Ma); (8) trachytes, comendites, and pantellerites of Changbaishan volcanic cone, Baitoushan period (1.12–0.81 Ma); (9) ignimbrites, pumices and ashes of the Changbaishan caldera, Bingchang–Baiyufeng–Baiguamiao periods (7854–825 kyr); (10) faults; (11) sampling sites and sample names.

plagioclase phenocrysts (sometimes megacrysts up to 1 cm). Plagioclase ($An_{74.3\text{-}79.1}Ab_{19.8\text{-}25.5}Or_{0.1\text{-}1.3}$) is the dominant phenocryst phase in these basalts. The basalt (sample B-19) from the upper part of the section of the shield volcano contains some isolated resorbed subphenocrysts of olivine (Fo = 74), which represent xenogenic phases out of equilibrium with the basaltic magma. It has been shown (Andreeva et al., 2020) that plagioclase is the first liquidus phase in the studied basalts. The groundmass minerals are represented by plagioclase, olivine (Fo = 43.2–56.4), titanaugite (#Mg = 0.64–0.70), ilmenite, titanomagnetite, fluorapatite and ferrocarbonate. There are also some "dry" and hydrous Fe-rich and Si-rich glasses present in the groundmass (Figure 3). Si-rich glass is characterized by the following composition: 70–77 wt% SiO_2, up to 9.4 wt% (Na_2O+K_2O) with a predominance of K_2O (ca. 7.5 wt%) over Na_2O (ca. 2.6 wt%), 10.5–14 wt% Al_2O_3, 0.2–2.2 wt% CaO, 0.6–2.2 wt% FeO and 0.9–1.5 wt% TiO_2 (Table 2). Fe-rich "dry" glass is globular and often finely crystallized. It contains 30–40 wt% SiO_2, up to 39 wt% FeO, 12.5–18.7 wt% TiO_2, up to 7.4 wt% P_2O_5 and up to 2.0 wt% SO_3 (Table 2). Hydrous Fe-rich glass is located in an interstitial position and sometimes has a globular morphology. It contains from 48 to 55 wt% SiO_2, 18–25 wt% FeO, 8–15 wt% MgO, 0.7–1.6 wt% Al_2O_3 and 0.9–1.7 wt% CaO, while the total alkalis do not exceed 0.4 wt% (Table 2). Water content is estimated by the difference from a constant sum of 100% of major oxide components in these glasses, leading to values of 10–15 wt% of H_2O, as shown by Andreeva et al. (2020).

The interstitial ferrocarbonate of the groundmass is characterized by distinct or weakly expressed concentric zonation

TABLE 1 Chemical composition (wt%) of basalts from Wangtian'e shield volcano, and the results of isotope analysis of oxygen and carbon (‰) of their groundmass.

Sample	B-15	B-16	B-17	B-18	B-19
SiO_2	48.66	50.10	49.38	48.93	48.66
TiO_2	3.30	3.08	3.22	3.52	2.44
Al_2O_3	15.80	14.00	15.39	15.64	18.51
Fe_2O_{3tot}	13.14	13.53	12.73	12.71	9.62
MnO	0.17	0.20	0.17	0.19	0.13
MgO	2.74	3.66	2.40	2.81	2.98
CaO	8.17	7.65	8.54	8.61	9.62
Na_2O	3.68	3.56	3.20	3.59	3.17
K_2O	1.54	1.75	1.48	1.47	1.09
P_2O_5	0.71	1.19	0.36	0.56	0.36
LOI	1.26	0.45	2.34	1.18	2.66
Total	99.17	99.17	99.21	99.21	99.24
$\delta^{18}O$ (m), ‰	19.38	20.25	19.72	19.56	—
$\delta^{13}C$ (m), ‰	−4.03	−6.84	−5.28	−3.53	—

Note: Fe_2O_{3tot}—total iron oxide content; m—rock groundmass. LOI— loss on ignition. Dashes mean not analysed.

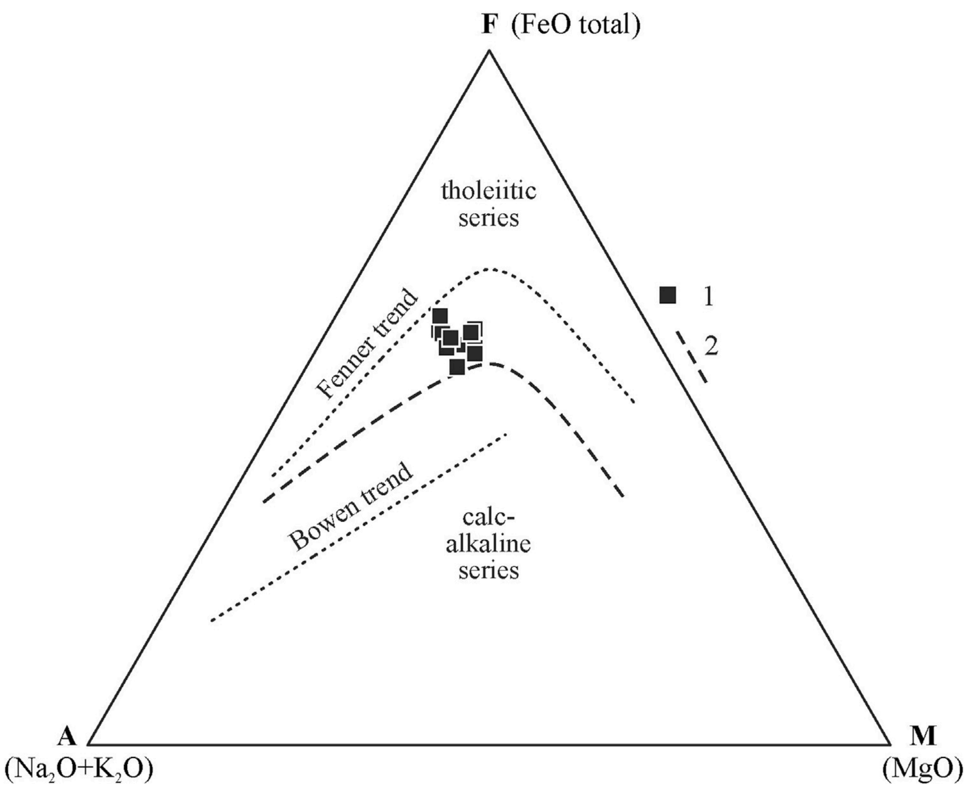

FIGURE 2
AFM diagram [(Na_2O+K_2O)−FeO_{tot}−MgO)] for rocks of Wangtian'e volcano. (1) Shield volcano of the Changbai period; (2) line between tholeiitic and calc-alkaline series by (Irvine and Baragar, 1971). Arrows indicate the Fenner and Bowen trends of fractional crystallization.

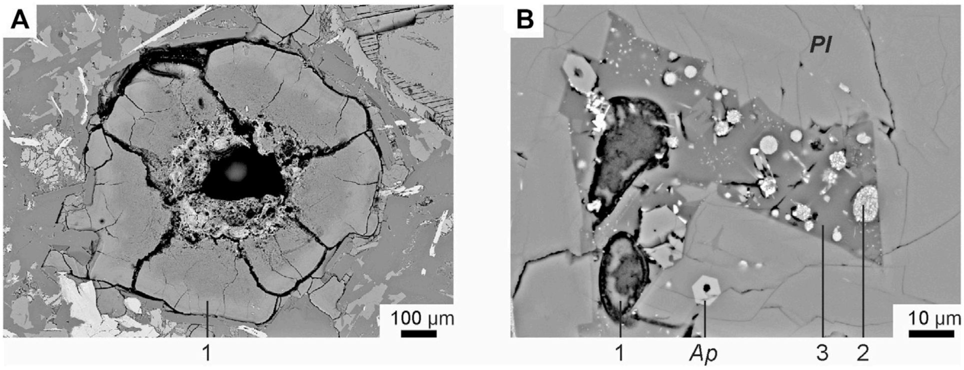

FIGURE 3
Backscattered electron images of groundmass glasses of tholeiitic basalts from Wangtian'e shield volcano (Andreeva et al., 2020): **(A)** groundmass water-bearing Fe-rich glass; **(B)** groundmass Si-rich glass with Fe-rich globules. (1) Water-bearing Fe-rich glass; (2) "dry" Fe-rich glass; (3) "dry" Si-rich glass. Mineral symbols: Ap—apatite, Pl—plagioclase.

TABLE 2 Chemical composition (wt%) of groundmass glasses and glasses in ferrocarbonates from Wangtian'e tholeiitic basalts.

Component	Groundmass "dry" Fe-rich glass		Groundmass "dry" Si-rich glass		Groundmass hydrous Fe-rich glass		Si-rich glass in siderite	
	B-19-2	B-19-5	B-19-8	B-19-11	B-19-15	B-19-16	B-16-4	B-16-5
SiO_2	32.29	30.12	71.81	73.57	48.42	52.41	68.49	68.1
TiO_2	6.31	12.50	0.59	2.70	0.13	0.04	0.63	0.63
Al_2O_3	1.94	1.02	13.68	10.32	1.42	0.90	13.92	14.17
FeO_{tot}	30.71	39.34	2.24	3.29	26.10	18.71	1.41	1.52
MnO	0.68	0.59	0.15	0.07	0.11	0.09	0.03	0.04
MgO	2.16	1.86	0.22	0.12	8.03	15.15	0.07	0.09
CaO	12.26	8.15	2.16	1.30	1.70	0.91	0.37	0.42
Na_2O	1.04	0.30	2.20	1.60	0.12	0.08	2.62	3.03
K_2O	1.06	0.17	5.99	5.23	0.08	0.39	7.41	7.47
P_2O_5	8.03	4.21	0.11	0.53	0.00	0.00	0.14	0.2
SO_3	1.26	2.01	0.05	0.15	0.02	0.02	—	—
ZrO_2	0.15	0.48	0.03	0.09	0.01	0.01	—	—
Cl	0.27	0.12	0.05	0.12	0.03	0.00	0.04	0.04
F	—	—	0.07	0.04	—	—	—	—
Ce_2O_3	0.37	0.31	0.03	0.15	0.07	0.01	—	—
Total	98.99	101.49	99.36	99.23	86.36	88.79	95.15	95.72

Note. FeO_{tot} is total iron oxide content. Dashes mean not analyzed.

(Figures 4A, B; Table 3). It contains inclusions of plagioclase, pyroxene, olivine, apatite and Si-rich glass (Figures 4C, D; Table 2). Ferrocarbonate is also found as crystalline inclusions in plagioclase; like the groundmass ferrocarbonate, it is characterized by 60–75 wt% $FeCO_3$, 14–32 wt% $MgCO_3$, 2–12 wt% $CaCO_3$, and up to 1.5 wt% $MnCO_3$ (Table 3).

4 Materials and methods

4.1 Analytical techniques

All sampled rocks from southeastern section of the Wangtian'e shield volcano (samples B-15, B-16, B-17, B-18,

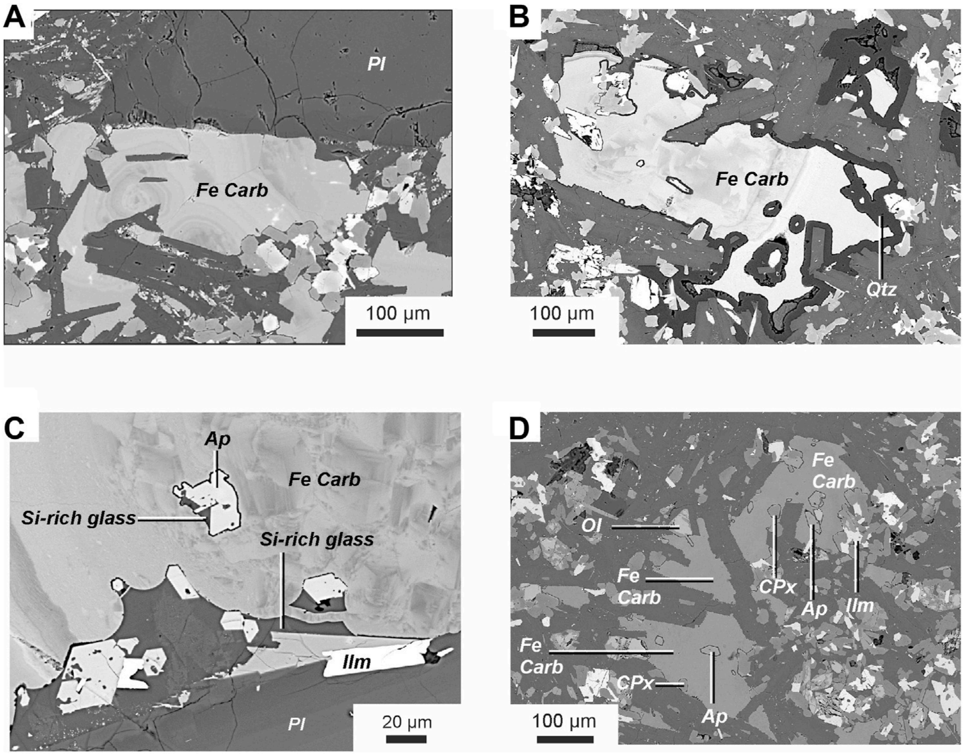

FIGURE 4
Backscattered electron images of ferrocarbonates and the ferrocarbonate-hosted inclusions. Phase symbols: *Pl*—plagioclase, *Fe Carb*—ferrocarbonate, *Ap*—apatite, *Ol*—olivine, *CPx*—clinopyroxene, *Ilm*—ilmenite.

and B-19) were analyzed for their major oxide contents using an X-ray fluorescence spectrometer PW-2400 (IGEM RAS, Moscow, Russia, Andreeva et al., 2018; Andreeva et al., 2020). Glasses in homogenized melt inclusions, daughter mineral phases in inclusions, crystal inclusions and rock-forming minerals were analyzed using EPMA JXA-8200 JEOL microprobe equipped with five WD spectrometrs (IGEM RAS, Moscow, Russia) at an accelerating voltage of 20 kV and beam current on the Faraday cylinder of 20 nA for minerals and 10 nA for glasses. The beam diameter was 1 μm when minerals were analyzed and varied from 2 to 10 μm when glasses were analyzed, depending on the size of the inclusions. The standards were minerals of composition close to that of the analyzed phases. Corrections were calculated by the ZAF routine, using a proprietary JEOL software. Detailed measurement conditions are shown in the (Supplementary Table S1). Trace elements and REE in whole-rocks were analysed on an XII ICP-MS ThermoScientific ICP-MS spectrometer (IGEM RAS, Moscow, Russia) with an accuracy of 1%–3% relative.

Oxygen and carbon isotope compositions of the groundmass ferrocarbonates and plagioclase-hosted ferrocarbonates were analysed using a CF-IRMS DeltaV+ instrument (Thermo, Finnigan) with a GasBenchII configuration and PAL autosampler, after decomposition of hand-picked separates in phosphoric acid at 70°C (Institute of Geology of Ore Deposits, Petrography, Mineralogy and Geochemistry Russian Academy of Sciences, Moscow). The technique is described in detail by Nikiforov et al. (2021). Due to the low content of carbonates in the silicate matrix (1%–3%), the $\delta^{13}C$ and $\delta^{18}O$ values were measured at an estimated accuracy ±0.4% and ±0.8‰ (1 σ), respectively. Measured values of $\delta^{13}C$ and $\delta^{18}O$ are expressed relative to VPDB and VSMOW, respectively (Nikiforov et al., 2021). Calibration of $\delta^{13}C$ and $\delta^{18}O$ values on the VPDB and VSMOW scales was performed by measuring the NBS 19 and NBS 18 international standards in the same analytical series.

The oxygen isotope compositions of plagioclase phenocrysts were determined on carefully picked separates (Institute of Geology of Ore Deposits, Petrography, Mineralogy and Geochemistry Russian Academy of Sciences, Moscow). The analysis was carried out by laser fluorination (Sharp, 1990). The error in $\delta^{18}O$ determination was ±0.1‰ or better. The results given in per mil relative to V–SMOW standard were checked against measurements of NBS 28 (quartz) and UWG 2 (garnet) standards (Valley et al., 1995). The technique is described in detail by Dubinina et al. (2015).

The decarbonation reaction of the initial carbonate is calculated using the fractionation factor "calcite-CO_2" at 1,200°C (Scheele and Hoefs, 1992; Chacko and Deines, 2008).

Thermodynamic calculations were performed using the HCh software package (Shvarov, 2008). Nine component system (Al-C-Ca-Fe-H-Mg-Na-O-Si) was used for the thermodynamic calculations which takes into account 42 mineral phases, a gas solution (H_2O-CO_2-O_2-H_2-CH_4

TABLE 3 Composition (wt%) of groundmass ferrocarbonate, crystalline inclusions represented by ferrocarbonate, and ferrocarbonate globules in melt inclusions in plagioclase from basalts of Wangtian'e shield volcano.

Sample name	$MgCO_3$	$FeCO_3$	$CaCO_3$	$MnCO_3$	Total[a]
B-16-1	14.66	75.21	8.83	1.30	100
B-16-2	27.02	60.11	11.47	1.40	100
B-16-3	22.26	74.01	2.49	1.23	100
B-16-4	28.22	67.39	3.53	0.86	100
B-16-5	31.65	65.50	1.83	1.02	100
B-16-6	22.21	73.08	3.35	1.36	100
B-16-Line 1	17.15	69.24	12.42	1.19	100
B-16-Line 2	17.20	69.37	12.29	1.14	100
B-16-Line 3	20.53	67.21	11.13	1.13	100
B-16-Line 4	22.83	65.99	10.00	1.19	100
B-16-Line 5	22.37	67.14	9.33	1.16	100
B-16-Line 6	20.61	68.46	9.79	1.13	100
B-16-Line 7	19.42	70.50	8.83	1.25	100
B-16-Line 8	17.85	70.33	10.63	1.19	100
B-15-Line-1	21.13	69.28	7.96	1.64	100
B-15-Line-2	19.20	76.01	3.87	0.93	100
B-15-Line-3	18.24	77.42	3.43	0.92	100
B-15-Line-4	14.01	81.62	3.17	1.20	100
B-15-Line-5	13.30	82.44	3.09	1.17	100
B-15-Line-6	29.91	63.62	5.46	1.01	100
B-15-Line-7	19.30	75.70	4.06	0.94	100
B-15-Line-8	14.99	78.67	5.09	1.25	100
B-15-36	18.94	71.32	8.23	1.52	100
B-16-9	17.47	70.83	10.49	1.21	100
B-16-31	16.97	68.15	13.73	1.15	100
B-16-32	14.66	75.21	8.83	1.30	100
B-15-23	14.09	81.07	3.75	1.09	100
B-15-24	14.40	81.30	3.19	1.10	100
B-15-25	17.94	77.19	3.82	1.05	100
B-15-26	18.63	77.12	3.25	1.00	100
B-15-27	16.28	78.76	3.78	1.18	100

Note: B-16-1–B-16-6–composition of ferrocarbonate from rock groundmass; B-16-Line-1–B-16-Line-8–composition by profile of zoned ferrocarbonate from rock groundmass of the sample B-16; B-15-Line-1–B-15-Line-8–composition by profile of zoned ferrocarbonate from rock groundmass of the sample B-15; B-15-36–B-16-32–crystalline inclusions represented by ferrocarbonate in plagioclase of basalts; B-15-23–B-15-27–ferrocarbonate globules in melt inclusions from plagioclase of basalts.
[a]Total normalized to 100 wt%.

mixture) and a carbonate melt. The fugacity of the components of the gas mixture was calculated using the Peng-Robinson equation (e.g., Lopez-Echeverry et al., 2017). The stability of the liquid carbonate melt was defined in the $FeCO_3$-$MgCO_3$-$CaCO_3$ ternary system. Thermodynamic parameters for liquid carbonate end-members were taken from Zhao et al. (2019) and Kang et al. (2016). A silicate melt was not taken into account under the assumption that the association of eutectic minerals was sufficient to describe the liquid-solid phase equilibrium.

TABLE 4 Chemical composition (wt%) of glasses and globules of unheated plagioclase-hosted melt inclusions and their host plagioclase from Wangtian'e tholeiitic basalts.

Compo-nent	Host plagioclase		Melt inclusions										
			a		b		c		d			e	
	2	4	6	9	10	11	12	13	14	16	18	20	22
SiO_2	53.10	52.88	55.59	65.90	42.94	43.15	40.39	43.83	73.80	71.81	72.07	44.73	46.24
TiO_2	0.13	0.12	0.12	0.10	5.68	5.72	7.36	6.47	0.48	0.59	0.94	0.06	0.01
Al_2O_3	29.17	29.20	28.25	21.64	1.94	2.01	2.74	2.91	14.19	13.68	13.57	3.23	3.48
FeO_{tot}	0.59	0.62	0.72	0.64	24.16	23.41	26.10	23.35	1.26	2.24	1.66	21.16	25.02
MnO	dl	0.03	dl	dl	0.33	0.33	0.43	0.35	0.09	0.15	0.04	0.35	0.29
MgO	0.10	0.11	0.18	0.02	10.88	11.75	10.12	10.07	0.07	0.22	0.18	7.69	8.49
CaO	12.52	12.85	10.91	2.48	10.20	10.34	9.70	10.01	0.99	2.16	1.13	1.85	1.43
Na_2O	4.21	4.09	4.94	6.23	0.68	0.72	0.62	0.85	1.03	2.20	2.18	0.11	0.05
K_2O	0.31	0.29	0.51	5.50	0.43	0.37	0.42	0.71	4.69	5.99	5.90	0.48	0.11
P_2O_5	—	—	—	—	0.95	0.88	1.03	1.14	0.05	0.11	0.21	dl	0.02
SO_3	—	—	—	—	0.38	0.34	dl	dl	0.30	0.05	dl	dl	0.09
Cl	—	—	—	—	0.03	0.02	0.05	0.04	0.06	0.05	0.07	0.57	dl
F	—	—	—	—	—	—	—	—	0.02	0.07	0.44	—	—
Total	100.12	100.19	101.23	102.66	98.80	99.29	99.66	100.30	97.20	99.36	98.19	84.17[a]	85.40

Note: (a) zoned rim of melt inclusions; (6) outer zone, (9) inner zone; (b) (10, 11) Fe-rich silicate glass of melt inclusions; (c) (12, 13) fine-grained Fe-rich aggregate of melt inclusions; (d) (14–18) Si-rich globules; (e) (20, 22) hydrous Fe-rich globules. FeO_{tot} is total iron oxide content.
[a]Total is given without H_2O content, that amounts 3.97 wt% (Andreeva et al., 2020). Dl indicates values below detection limit. Dashes mean not analysed.

4.2 Techniques applied to study magmatic inclusions in minerals

The studied more than a hundred melt inclusions are partially or completely crystallized at room temperature, so we carried out experimental re-heating prior to analysis and estimation of the crystallization temperatures of the rock-forming minerals. For this purpose, we used muffle furnaces and a Linkam TS1500 high-temperature stage (Institute of Geology of Ore Deposits, Petrography, Mineralogy and Geochemistry Russian Academy of Sciences, Moscow). The temperature was controlled with a $Pt-Pt_{90}Rh_{10}$ thermocouple calibrated on the melting points of $K_2Cr_2O_7$ (T_m = 398°C), NaCl (T_m = 800°C), and Au (T_m = 1,064°C). The integrated error of the temperature measurements was estimated at ±10°C (Andreeva et al., 2018; Andreeva et al., 2020). The duration of re-heating experiments for melt inclusions in plagioclase in basalts were up to 10–15 min according to (Danyushevsky et al., 2002; Esposito, 2021).

The composition of the fluid phases was analyzed by Raman spectroscopy using a Renishaw spectrometer (Frumkin Institute of Physical Chemistry and Electrochemistry, Russian Academy of Sciences, Moscow, Andreeva et al., 2023). Raman spectra were recorded using the 405-nm line of a Nd:YAG laser at a power of <2 mW and a spectral resolution of ~2 cm^{-1}. The signal acquisition time was ~200 s. The spectra were recorded using a ×100 objective with a scattering cross-section of ~1 μm. The instrument was calibrated using an internal silicon wafer. Experimental spectra were decomposed into several components using Fityk software (Wojdyr M., 2010).

5 Results

5.1 Melt and fluid inclusions

Primary melt and fluid inclusions are recorded in the plagioclase of tholeiitic basalts from Wangtian'e volcano. The primary melt inclusions vary in size from 30 to 100 μm. They are partially or completely crystallized, and consist of anhydrous Fe-rich glass or fine-grained mineral aggregates composed of clinopyroxene, titanomagnetite, ilmenite, apatite and sulfides. Fe-rich glass and fine-grained mineral aggregates were analysed by electron microprobe using an expanded electron beam with a diameter of 10 μm. The compositions of Fe-rich glass and fine-grained mineral aggregates are similar and are characterized by high contents of FeO (up to 24 wt%), CaO (up to 10 wt%), MgO (12 wt%) and TiO_2 (up to 6 wt%) as well as low concentrations of Al_2O_3 (<2 wt%), Na_2O+K_2O (1 wt%), P_2O_5 (1 wt%) and SO_3 (0.3–0.4 wt%), with a SiO_2 content of 40–43 wt% (Table 4). The fine-grained mineral aggregates in the inclusions are interpreted as a crystallized Fe-rich melt. In addition, the inclusions contain wide zonal feldspar rims. The composition of these rims varies from the outer part towards the core of the inclusions from plagioclase ($An_{46-56}Ab_{39-47}Or_{4-7}$) to anorthoclase ($An_{13-13.5}Ab_{43-50}Or_{36-43}$). Globules of various compositions are

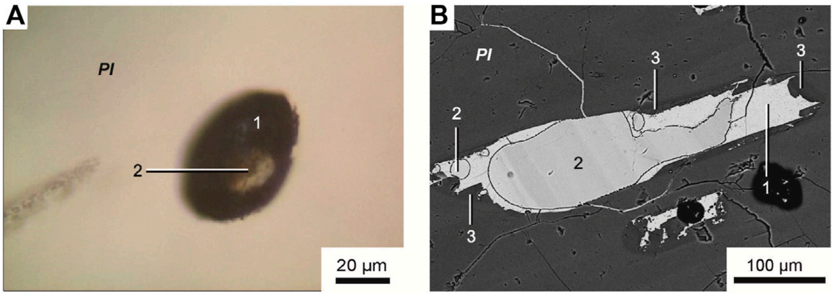

FIGURE 5
(A) Transmitted-light microphotograph and **(B)** backscattered electron image of unheated plagioclase-hosted melt inclusion. (1) Fine-grained Fe-rich aggregate, (2) ferrocarbonate globule, (3) feldspar rim.

TABLE 5 Chemical composition (wt%) of glasses of the homogenized melt inclusions in the host plagioclase from Wangtian'e tholeiitic basalts.

Sample	B-19-1	B-19-2	B-19-3	B-19-4	B-19-5	B-15-1	B-15-2	B-15-3	B-15-4	B-15-5
Homogenization, T°C	1,190	1,190	1,190	1,180	1,170	1,195	1,195	1,200	1,205	1,205
SiO_2	48.78	48.15	48.63	50.33	48.36	49.69	49.47	51.13	51.69	54.28
TiO_2	3.64	3.47	3.60	2.87	3.83	3.00	3.14	2.79	2.49	1.66
Al_2O_3	16.35	16.48	16.42	16.19	14.84	16.43	16.16	17.09	16.90	17.92
FeO_{tot}	11.71	12.09	11.85	11.41	12.34	11.00	10.83	9.47	8.91	8.62
MnO	0.22	0.13	0.16	0.09	0.12	0.19	0.05	0.11	0.10	0.07
MgO	4.33	4.57	4.46	3.95	4.19	4.49	4.44	4.36	3.69	3.58
CaO	8.50	8.51	8.67	8.08	8.81	9.04	9.03	8.79	8.95	8.68
Na_2O	3.14	3.00	2.99	2.98	2.86	3.56	3.52	4.10	3.85	3.12
K_2O	1.32	1.28	1.29	1.59	1.53	1.12	1.10	1.44	1.36	0.95
P_2O_5	0.57	0.61	0.60	0.43	0.65	0.43	0.45	0.34	0.44	0.24
SO_3	0.62	1.65	0.52	0.51	0.57	0.31	0.33	0.28	0.24	0.08
Cl	0.03	0.02	0.02	0.02	0.03	0.02	0.01	0.02	0.01	dl
F	0.17	0.11	0.26	0.07	0.12	0.08	0.11	0.13	dl	0.01
Total	99.34	100.05	99.39	98.53	98.22	99.44	98.71	100.04	98.69	99.30

Note: FeO_{tot}—total iron oxide. Dl indicates values below detection limit.

found in many inclusions. Among them, silicate and carbonate globules are identified. Silicate globules are represented by 1) hydrous Fe-rich glass; 2) hydrous Si-rich glass; 3) anhydrous Si-rich glass (Table 4). The composition of these globules is similar to that of the Si-rich and Fe-rich groundmass glasses. As shown in previous studies (Andreeva et al., 2020), the hydrous Fe-rich glasses contain at least 4 wt% H_2O. The sum of major oxides in these globules and in the groundmass glasses indicate H_2O concentrations of about 10–15 wt%. Carbonate droplets (Figures 5A, B) in the melt inclusions have compositions similar to the ferrocarbonates found in the groundmass (Table 3).

Homogenization experiments performed on the melt inclusions show that most of the inclusions containing carbonate globules are decrepitated on heating. Inclusions that do not contain globules are homogenized in the temperature range of T = 1,180°C–1,200°C. After heating, the inclusions contain glass ± sulfide globule ± gas bubble. The glass composition corresponds to basalt with high contents of FeO (11.5–12.5 wt%) and TiO_2 (up to 4 wt%) (Table 5). The total alkali content reaches 5 wt%. Glass is also characterized by high concentrations of P_2O_5 (up to 0.8 wt%) and SO_3 (up to 0.6 wt%) (Table 5). The H_2O content is low and varies from 0.1 to 0.8 wt% (Andreeva et al., 2020). The formation of sulfide globules during the heating experiments (T = 1,180°C–1,200°C) as well as the presence of sulfide globules in minerals from this rock suggests that the melt exsolved into immiscible silicate and sulfide liquids. Similar results were obtained on melt inclusions in minerals of various rock types from Changbaishan volcano (Andreeva et al., 2019).

Primary fluid inclusions of one phase carbon dioxide coexisting with primary melt inclusions are found in plagioclase phenocrysts (Figures 6A, B). More than 30 fluid inclusions were studied. The positions of the characteristic CO_2 peaks (Fermi dyads) in the

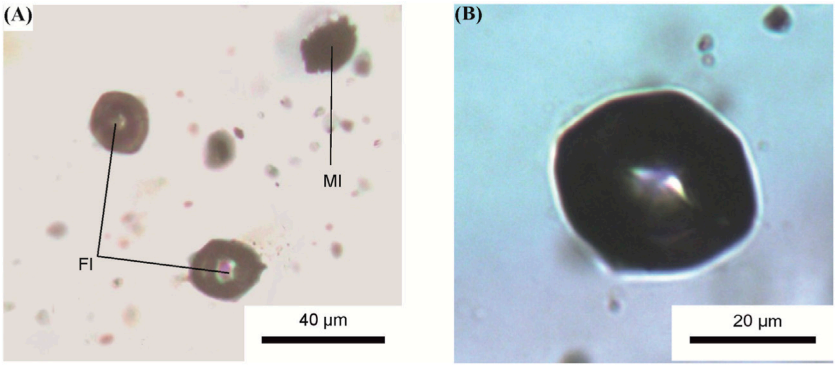

FIGURE 6
Transmitted-light microphotographs **(A,B)** of primary CO_2 fluid inclusions coexisting with primary melt inclusions in plagioclase of tholeiitic basalts from Wangtian'e shield volcano. **(A)** Primary melt and fluid inclusions. FI—fluid inclusions, MI—melt inclusions; **(B)** Primary CO_2 one phase fluid inclusion.

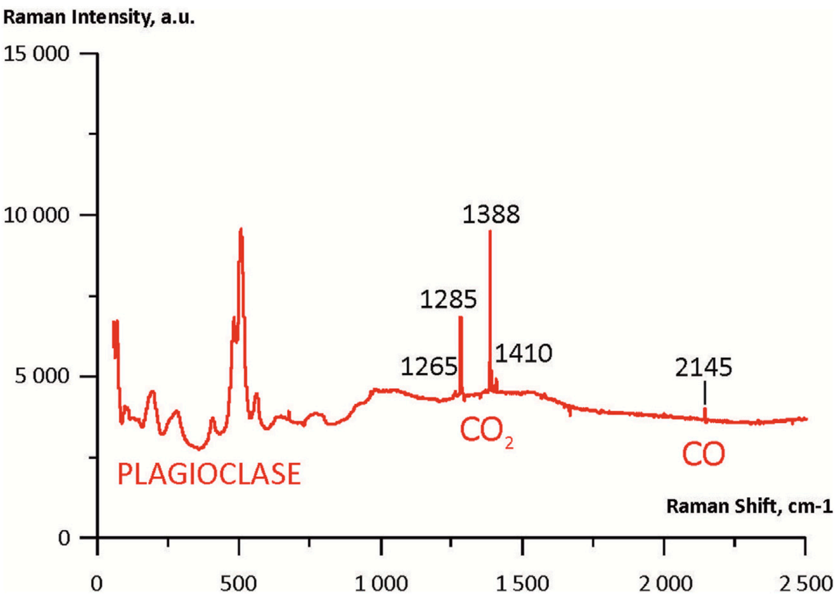

FIGURE 7
Micro-Raman spectra of plagioclase-hosted fluid inclusions.

inclusions were determined by Raman spectroscopy. The peak positions correspond to the range of 1,283.2 and 1,386.6 cm^{-1}–1,285.2 and 1,388.6 cm^{-1} (Figure 7; Supplementary Table S2). The density (ρ) of the CO_2 in the fluid inclusions is calculated according to the following (Equation 1) (Wang et al., 2011):

$$\rho = 47513.64243 - 1374.824414 ^* \Delta + 13.25586152 ^* \Delta^2 - 0.04258891551 ^* \Delta^3 \quad (1)$$

where Δ is the distance between the Fermi dyads. The calculated CO_2 density is equal to 0.23–0.33 g/cm^3. The pressures calculated from the pressure-volume-temperature parameters of CO_2 (Bottinga and Richet, 1981) correspond to the range of 0.1 ± 0.01 GPa. As was shown by Remigi et al. (2021), below the critical density gas-like CO_2 (d = 0.34 g/cm^3) narrower bands showed progressively increasing asymmetric profiles, resulting in more challenging to obtain a sufficiently accurate fitting of central positions. However we identified quite symmetric peaks.

5.2 Ferrocarbonate speciation and composition

Ferrocarbonate minerals are found in the groundmass of tholeiitic basalts from the Wangtian'e shield volcano, occurring as crystalline inclusions in plagioclase, and also as globules in melt inclusions in the plagioclase. The ferrocarbonate of the groundmass has an interstitial position and is characterized by distinct or weakly expressed concentric zonation (Figures 4A, B).

TABLE 6 Oxygen and carbon isotopic composition (‰) of ferrocarbonate inclusions in plagioclase and oxygen isotopic composition (‰) of the host plagioclase.

Sample	$\delta^{18}O$ of ferrocarbonate inclusions in plagioclase, ‰	$\delta^{13}C$ of ferrocarbonate inclusions in plagioclase, ‰	$\delta^{18}O$ of plagioclase, ‰
B-15	19.4	−3.78	6.1
B-19	17.2	−9.20	6.1

It contains 60–75 wt% $FeCO_3$, 14–32 wt% $MgCO_3$, 2–12 wt% $CaCO_3$, and up to 1.5 wt% $MnCO_3$ (Table 3). The groundmass ferrocarbonate contains inclusions of plagioclase, pyroxene, olivine, apatite, and Si-rich glass. Crystalline inclusions of apatite in ferrocarbonate are often surrounded by Si-rich glass (Figures 4C, D). Sometimes, quartz rims are observed at the boundary between apatite inclusions and host ferrocarbonate (Figures 4B). In addition, quartz rims are found at the boundaries between ferrocarbonates and various silicate minerals (plagioclase, clinopyroxene) and ore minerals (ilmenite, titanomagnetite). The Si-rich glass in ferrocarbonates (Figures 4C, D), intergrown with apatite has a composition similar to the Si-rich glass of the rock groundmass. It contains 68.0–70.0 wt% SiO_2, up to 0.6 wt% TiO_2, 1.4–1.8 wt% FeO and 12.8–13.9 wt% Al_2O_3. The total alkali content reaches 10.5 wt% with a significant predominance of K_2O (up to 7.5 wt%) over Na_2O (up to 3.0 wt%) (Table 2). Ferrocarbonates are also found as crystalline inclusions in plagioclase. The ferrocarbonate inclusions have a composition similar to the groundmass ferrocarbonates (Table 3; Figures 5A, B).

Globules in the un-reheated melt inclusions (Figures 5A, B) were analysed using Raman spectroscopy method and the electron microprobe. The Raman peak position corresponds to the CO_3^{2-} ion (1,091 cm^{-1}). Compositionally, these globules are characterized by 77.1–81.1 $FeCO_3$, 14.1–18.6 $MgCO_3$, 3.2–3.8 wt% $CaCO_3$ and 1.0–1.2 wt% $MnCO_3$ (Table 3).

5.3 Oxygen and carbon isotope composition

Oxygen and carbon isotope composition in carbonate minerals was determined in samples of tholeiitic basalts from the Wangtian'e shield volcano (samples B-15, B-16, B-17, B-19). The studied basalts contain from 1 to 3 vol% carbonate, which is expressed both among the groundmass minerals and as inclusions in plagioclase. The $\delta^{18}O$ values in the carbonates from bulk rock samples vary in the range +19.4 to +20.3‰ (relative to VSMOW), and $\delta^{13}C$ values vary from −3.5 to −6.8‰ (relative to VPDB) (Table 1). In addition, we studied the oxygen and carbon isotope composition of ferrocarbonate inclusions in plagioclase (Table 6). For two plagioclase-hosted ferrocarbonate inclusions, we obtained closely similar $\delta^{18}O$ and $\delta^{13}C$ values (+17.2, +19.4‰ and −3.78, −9.20‰, respectively). Analyses of the silicate matrix of the same plagioclase samples both yield a $\delta^{18}O$ value of +6.1‰ (Table 6).

6 Discussion

6.1 Origin of ferrocarbonates

The isotope data obtained on basalts from the Wangtian'e volcano are sharply distinguished from the basaltic series of the Changbaishan volcano. Analyses of the bulk isotope composition of Changbaishan basalts yield $\delta^{18}O$ values of +5.6–+5.8‰ (Dubinina et al., 2020). The basalts of Wangtian'e volcano contain up to 3 vol% of carbonates, which clearly affects the isotope compositions of bulk rock samples and ferrocarbonate inclusions contained in the plagioclase of these rocks. The $\delta^{18}O$ isotope characteristics (+17.2–+20.3‰), as well as the $\delta^{13}C$ values (−3.5 to −9.20‰), show that the groundmass ferrocarbonate as well as one sample of an inclusion in plagioclase, are both of sedimentary origin. The carbon isotope composition clearly indicates isotopic disequilibrium and indicates the mechanism of carbonate decomposition. The $\delta^{18}O$ (relative to VSMOW) versus $\delta^{13}C$ (relative to VPDB) diagram (Figure 8) shows that the compositional points of the studied basalts lie on the line representing the decarbonation reaction of the initial sedimentary carbonate at high temperatures. It can be seen from Figure 8 that 4 to 0.4 vol% of the carbonate remains during decarbonation of the initial sedimentary carbonate. Such an effect is regularly observed during the interaction of basaltic melts with carbonates derived from host rocks (e.g., Dubinina et al., 2019; Nikiforov et al., 2021; Nosova et al., 2021).

According to Sheet 1 of the Northeast Asia Geodynamics Map at a scale of 1:5,000,000, (USGS, 2004), the basement of the Changbaishan volcanic field is made up of marbles and limestones belonging to the Archean-Proterozoic granite-gneisses of the Sino-Korean craton. Under the Wangtian'e shield volcano on the southern margin of the Changbaishan volcanic field, the Paleoproterozoic Sangwon sedimentary basin reaches a thickness of several thousand meters. It is composed mainly of detrital rocks, marbles and limestones. Our studies show that basaltic magmas rising to the Earth's surface passed through these marbles and limestones, and assimilated the ancient country rocks. At high temperatures, the marbles and limestones underwent partial decomposition with the release of CO_2. The study of melt inclusions containing ferrocarbonate globules indicates that contamination with sedimentary carbonates occurred simultaneously or even earlier than the crystallization of plagioclase in the basaltic melt. The study of CO_2 fluid inclusions in plagioclase indicates that the contamination of basaltic melts with marbles occurred at a pressure of 0.1 ± 0.01 GPa at a depth of about 4 km.

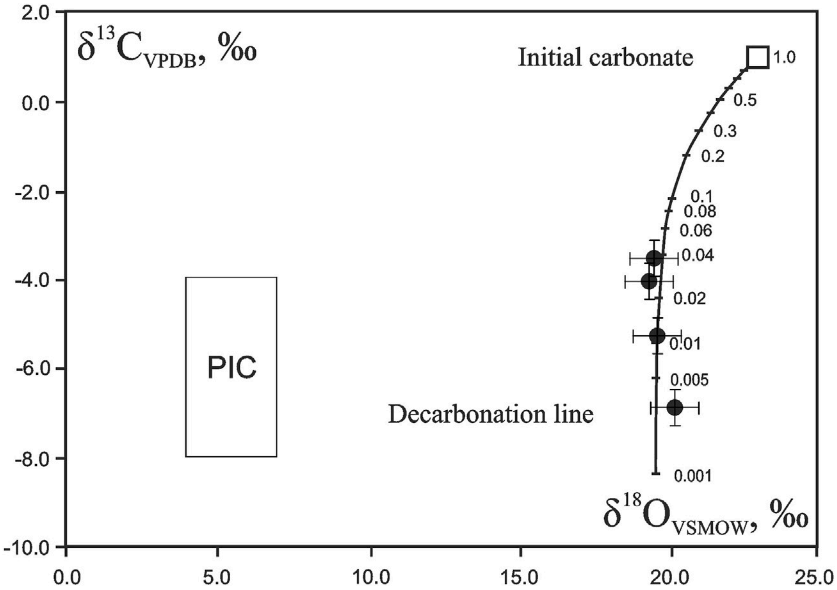

FIGURE 8
$\delta^{13}C$ (‰) versus $\delta^{18}O$ (‰) diagram illustrating evolution of isotopic compositions during decarbonation process associated with basalt formation in Wangtian'e shield volcano. The decarbonation line is calculated using the fractionation factors "calcite-CO_2" for 1,200°C (Scheele and Hoefs, 1992; Chacko and Deines, 2008). PIC represents the compositional field of primary igneous carbonatites according to (Taylor et al., 1967).

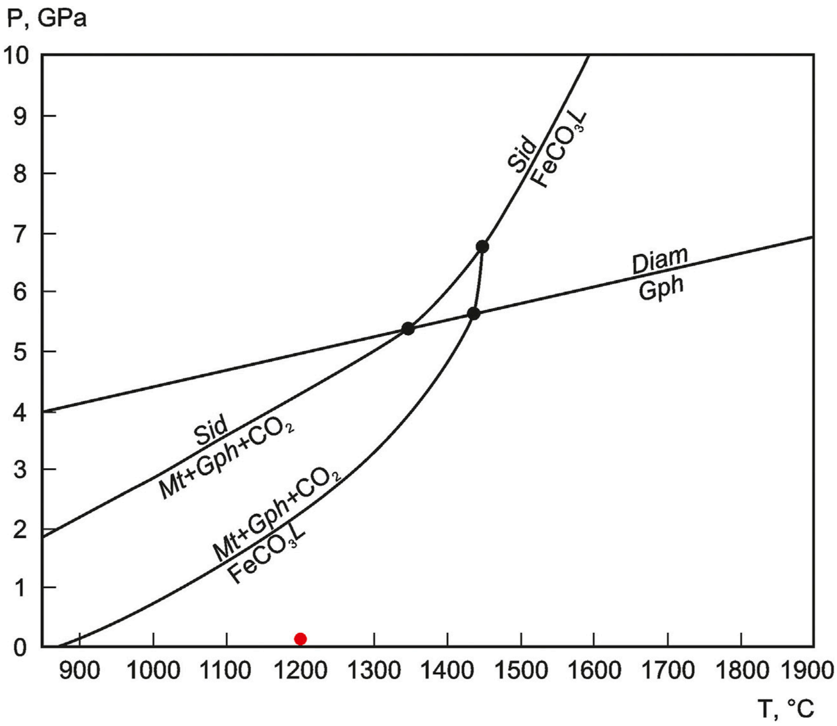

FIGURE 9
P (GPa) versus T (°C) phase diagram illustrating melting reactions of siderite according to the experimental data of Kang et al. (2015). Red point represents T-P parameters of Wangtian'e magmatic chamber. Phase symbols: Sid—siderite, $FeCO_3L$—siderite melt, Mt—magnetite, Gph—graphite, Diam—diamond.

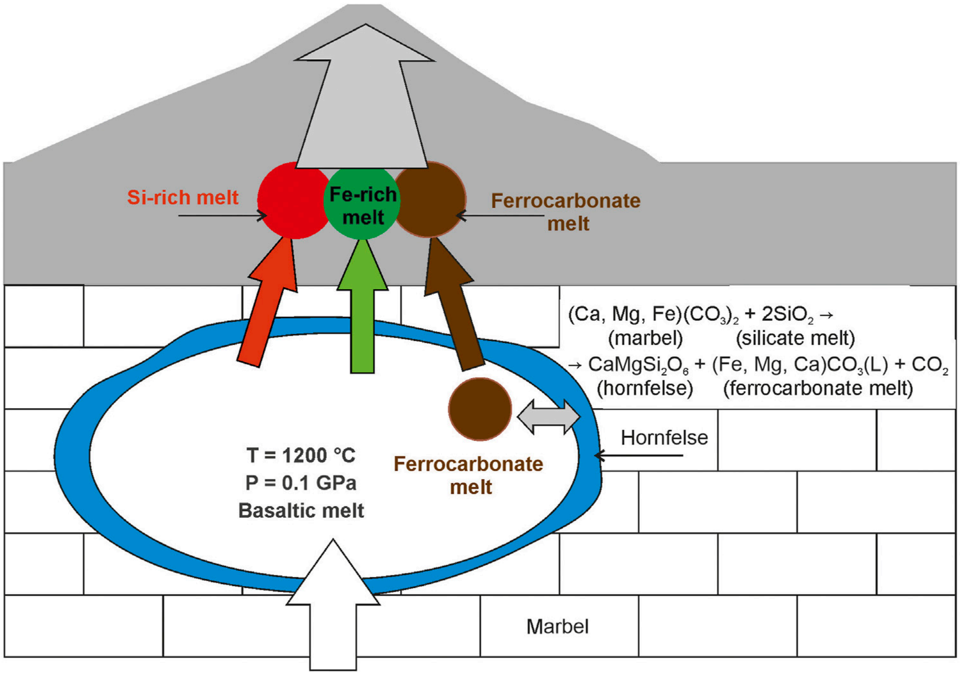

FIGURE 10
Geochemical model of ferrocarbonate formation in Wangtian'e shield basalts showing magma chamber processes: reaction between basaltic melt and host marbel with ferrocarbonate melt production, silicate-ferrocarbonate and silicate-silicate liquid immiscibility.

6.2 Silicate-carbonate immiscibility

The different ferrocarbonate phases in the Wangtian'e tholeiitic basalts occur as groundmass minerals, crystalline inclusions in plagioclase and also as globules in melt inclusions, suggesting that ferrocarbonate minerals crystallized from a ferrocarbonate melt. This is also supported by the occurrence of inclusions of plagioclase, pyroxene, olivine, apatite, and Si-rich glass in ferrocarbonates. According to the experimental phase diagram of Kang et al. (2015), incongruent melting of ferrocarbonate (siderite) occurs with decreasing pressure and temperature, with the formation of a ferrocarbonate liquid (Figure 9). At a temperature of T = 1,200°C and pressure p = 0.1 ± 0.01 GPa, a ferrocarbonate melt exists in the system illustrated on Figure 9. The ferrocarbonate melt can be formed by the interaction of the basaltic melt with host marbles and limestones (Equation 2), according to the following reaction:

$$CaMg(CO_3)_2 + FeCO_3 + 2SiO_2 = CaMgSi_2O_6 + FeCO_3\ (melt) + 2CO_2 \quad (2)$$

where $CaMg(CO_3)_2$ is dolomite from limestones, $FeCO_3$ corresponds to iron content in limestone carbonates, SiO_2 is a component of silicate melt; and carbon dioxide gas (CO_2) is liberated and diopside hornfelses ($CaMgSi_2O_6$) with carbonate liquid $FeCO_3$ (melt) which are formed in the magma chamber. At the same time, ferrocarbonate melt coexisted in the magma chamber together with the silicate melt as immiscible liquids. Due to the silicate-carbonate immiscibility and kinetic effect, the ferrocarbonate melt could remained isotopically isolated from the silicate melt.

The stability of the ferrocarbonate melt at temperature and pressure is confirmed by thermodynamic calculations whereby a solidus association of minerals is used instead of a silicate melt. The composition of the initial basaltic melt is taken from the results of the study of melt inclusions in plagioclase (sample B-19). The marble composition is selected from Liu and Jin (2022). Calculations of the interaction between marbles and the solidus association of basalt minerals at T = 1,200°C and pressure p = 0.1 ± 0.01 GPa show that a ferrobasaltic melt is stable in the presence of gaseous carbon dioxide. The calculated composition contains 73.2 wt% $FeCO_3$, 24.0 wt% $MgCO_3$ and 3 wt% $CaCO_3$, which is in good agreement with the observed data. Such a ferrocarbonate melt exists in equilibrium with quartz, wollastonite, diopside and plagioclase. This mineral association corresponds to hornfelses that are formed due to marble assimilation.

The occurrence of quartz rims at the boundary between ferrocarbonate inclusion and the host silicate minerals, apatite, and ilmenite indicates that a certain amount of SiO_2 was exsolved from the ferrocarbonate melt upon the inclusion cooling. As the ferrocarbonate cooled and crystallized, the silicic melt initially dissolved in the ferrocarbonate melt was "squeezed" out, forming rims on the inclusion walls.

As shown earlier (Andreeva et al., 2020), the separation of a FeO-enriched (up to 15 wt%) melt into immiscible Fe-rich and Si-rich liquids occurs at the late stages of basalt crystallization upon cooling. Similar processes were described by Lima and Esposito (2023) and Lino et al. (2023). The presence of Si-rich glass in ferrocarbonates suggests that ferrocarbonate mineral crystallization occurred during the final stages of the basalt formation in the Wangtian'e shield volcano upon the magma cooling.

7 Geochemical model

The obtained results lead us to develop a geochemical model for the formation of ferrocarbonates in the basalts of the Wangtian'e shield volcano. As basaltic melts ascended to the surface at a depth of about 4 km, they became to be contaminated with the crustal marbles. The reaction of basaltic melts with marble can be written as follows:

Ca(Mg, Fe) $(CO_3)_2$ (marble) + $2SiO_2$ (silicate melt) → $CaMgSi_2O_6$ (hornfels) + (Fe, Mg, Ca) CO_3 (L) (ferrocarbonate melt) + CO_2 (fluid) (3), where Ca(Mg, Fe) $(CO_3)_2$ is marble component, SiO_2 is silica in the basaltic melt; $CaMgSi_2O_6$ is diopside in hornfels and (Fe, Mg, Ca) CO_3 is ferrocarbonate melt, and CO_2 is fluid component. As a result, diopside hornfelses were formed on the walls of the magma chamber, carbon dioxide exsolved as fluid from the system, and basaltic and ferrocarbonate melts coexisted in the chamber as immiscible (Figure 10). The evolution of the basaltic melt follows the Fenner trend of fractional crystallization, as shown earlier (Figure 2; Andreeva et al., 2020). With decreasing temperature and pressure, the basaltic melt was exsolved to immiscible Fe-rich and Si-rich liquids. At the same time, the ferrocarbonate melt independently crystallized. Thus, three immiscible liquids (Fe-rich, Si-rich, and ferrocarbonate) crystallized during the final stages of tholeiite basalt formation (Figure 10).

8 Conclusion

Ferrocarbonates (or Fe-rich carbonate minerals) are found as minerals in the groundmass of Wangtian'e basalts, and as crystalline inclusions and globules in melt inclusions in the plagioclase. The chemical composition and speciations of ferrocarbonates indicate that they are a product of crystallization of a ferrocarbonate melt. Based on these inclusions we infer that the crystallization of basalts occurred in a near-surface magma chamber at a temperature of 1,180°C–1,200°C and a pressure of 0.1 GPa. Two different silicate-silicate and silicate-carbonate liquid immiscibility processes are distinguished and carbonate immiscibility modeled thermodynamically. The analyzed $\delta^{18}O$ and $\delta^{13}C$ values indicate that ferrocarbonates are of sedimentary origin, undergoing processes of partial decomposition of carbonate and melt-to-carbonate interactions. The isotopically disequilibrium of the ferrocarbonate melt and the host basaltic magma occurred during the interaction of basaltic magma with host crustal marbles. The mineral phase diagram and thermodynamic calculations show that the ferrocarbonate melt is thermodynamically stable at a temperature of 1,200°C and a pressure of 0.1 GPa. Other components of carbonates such as magnesium and calcium are converted to silicates (diopside and wollastonite) in the contact hornfelse rock upon magma cooling.

Data availability statement

The raw data supporting the conclusion of this article will be made available by the authors, without undue reservation.

Author contributions

OA: Conceptualization, Investigation, Methodology, Writing–original draft. ED: Data curation, Investigation, Methodology, Writing–original draft. IA: Investigation, Methodology, Writing–original draft. VVY: Conceptualization, Supervision, Writing–original draft. ABy: Investigation, Methodology, Software, Writing–original draft. ABo: Conceptualization, Supervision, Writing–original draft. J-QJ: Investigation, Writing–original draft. XZ: Investigation, Writing–original draft. EK: Methodology, Writing–original draft. SB: Methodology, Writing–original draft. AA: Methodology, Writing–original draft.

Funding

The author(s) declare financial support was received for the research, authorship, and/or publication of this article. This study was financially supported by the Russian Science Foundation, Project No. 22-17-00033.

Acknowledgments

The manuscript was greatly improved by reviews from Tong Hou, Rosario Esposito and the Editor Simona Ferrando.

Conflict of interest

The authors declare that the research was conducted in the absence of any commercial or financial relationships that could be construed as a potential conflict of interest.

Publisher's note

Supplementary material

The Supplementary Material for this article can be found online at: https://www.frontiersin.org/articles/10.3389/feart.2023.1306460/full#supplementary-material

References

Andreeva, I. A., Yarmolyuk, V. V., and Borisovsky, S. E. (2023). Magma composition and formation conditions of alkali-salic rocks of the Early Mesozoic Adaatsag bimodal association of the Kharkhorin rift zone of Central Asia (data from the study of melt inclusions in minerals). *Dokl. Earth Sci.* 509, 435–442. doi:10.1134/S1028334X22602048

Andreeva, O. A., Andreeva, I. A., and Yarmolyuk, V. V. (2019). Effect of redox conditions on the evolution of magmas of Changbaishan Tianchi volcano, China-North Korea. *Chem. Geol.* 508, 225–233. doi:10.1016/j.chemgeo.2018.09.039

Andreeva, O. A., Andreeva, I. A., Yarmolyuk, V. V., Ji, J.-Q., Zhou, X., and Borisovskii, S. E. (2020). Silicate liquid immiscibility as a result of Fenner-type crystal fractionation of Wangtian'e tholeiitic melts, Northeast China. *Petrology* 28 (4), 357–373. doi:10.1134/s0869591120040025

Andreeva, O. A., Yarmolyuk, V. V., Andreeva, I. A., and Borisovskiy, S. E. (2018). Magmatic evolution of Changbaishan Tianchi volcano, China-North Korea: evidence from mineral-hosted melt and fluid inclusions. *Petrology* 26 (5), 515–545. doi:10.1134/s0869591118050028

Andreeva, O. A., Yarmolyuk, V. V., Andreeva, I. A., Ji, J.-Q., and Li, W. R. (2014). The composition and sources of magmas of Changbaishan Tianchi volcano (China-North Korea). *Dokl. Earth Sci.* 456 (I), 572–578. doi:10.1134/s1028334x14050213

Andreeva, O. A., Yarmolyuk, V. V., Savatenkov, V. M., Andreeva, I. A., Lebedev, V. A., Ji, J.-Q., et al. (2022). Tholeiitic and alkaline basaltic lavas of Wang-Tian'e and Changbaishan volcanoes (northeastern China): timing and genetic relationship. *Dokl. Earth Sci.* 506 (I), 641–649. doi:10.1134/s1028334x22600323

Blythe, L. S., Deegan, F. M., Freda, C., Jolis, E. M., Masotta, M., Misiti, V., et al. (2015). CO_2 bubble generation and migration during magma - carbonate interaction. *Contrib. Mineral. Petrol.* 169, 42. doi:10.1007/s00410-015-1137-4

Borisova, A., and Bohrson, W. A. (2023). How is carbonate crust digested by magma? *Front. Earth Sci.* 11, 1186207. doi:10.3389/feart.2023.1186207

Bottinga, Y., and Richet, P. (1981). High pressure and temperature equation of state and calculation of the thermodynamic properties of gaseous carbon dioxide. *Am. J. Sci.* 281, 615–660. doi:10.2475/ajs.281.5.615

Chacko, T., and Deines, P. (2008). Theoretical calculation of oxygen isotope fractionation factors in carbonate systems. *Geochim. Cosmochim. Acta* 72, 3642–3660. doi:10.1016/j.gca.2008.06.001

Danyushevsky, L. V., McNeill, A. W., and Sobolev, A. V. (2002). Experimental and petrological studies of melt inclusions in phenocrysts from mantle-derived magmas: an overview of techniques, advantages and complications. *Chem. Geol.* 183, 5–24. doi:10.1016/s0009-2541(01)00369-2

Deegan, F. M., Troll, V. R., Freda, C., Misiti, V., Chadwick, J. P., McLeod, C. L., et al. (2010). Magma-carbonate interaction processes and associated CO_2 release at Merapi volcano, Indonesia: insights from experimental petrology. *J. Petrol.* 51, 1027–1051. doi:10.1093/petrology/egq010

Dubinina, E. O., Andreeva, O. A., Avdeenko, A. S., Andreeva, I. A., and Ji, J.-Q. (2020). Oxygen isotope fractionation between phenocrysts and melt: equilibrium estimation for the alkaline lavas of Changbaishan volcano (northeast China). *Petrology* 28 (3), 287–300. doi:10.1134/s0869591120030030

Dubinina, E. O., Aranovich, L. Y., van Reenen, D. D., Avdeenko, A., Varlamov, D., Shaposhnikov, V., et al. (2015). Involvement of fluids in the metamorphic processes within different zones of the Southern Marginal Zone of the Limpopo complex, South Africa: an oxygen isotope perspective. *Precambrian Res.* 256, 48–61. doi:10.1016/j.precamres.2014.10.019

Dubinina, E. O., Filimonova, L. G., and Kossova, S. A. (2019). Isotope ($\delta^{34}S$, $\delta^{13}C$, $\delta^{18}O$) compositions of disseminated sulfide mineralization in igneous rocks of the Dukat ore deposit (Northeastern Russia). *Geol. Ore Depos.* 61 (1), 38–49. doi:10.1134/s1075701519010033

Esposito, R. (2021). "A protocol and review of methods to select, analyze and interpret melt inclusions to determine pre-eruptive volatile contents of magmas," in *Fluid and melt inccusions – applications to geologic processes*. Editor R. Raeside (Canada: MAC) 49, 163–193.

Fan, Q., Liu, R., Li, D., and Li, Q. (1999). Significance of K-Ar age of bimodal volcanic rocks at Wangtian'e volcano, Changbaishan area. *Chin. Sci. Bull.* 44 (7), 660–663. doi:10.1007/bf03182731

Freda, C., Gaeta, M., Misiti, V., Mollo, S., Dolfi, D., and Scarlato, P. (2008). Magma-carbonate interaction: an experimental study on ultrapotassic rocks from Alban Hills (Central Italy). *Lithos* 101, 397–415. doi:10.1016/j.lithos.2007.08.008

Fulignati, P., Kamenetsky, V. S., Marianelli, P., Sbrana, A., and Mernagh, T. P. (2001). Melt inclusion record of immiscibility between silicate, hydrosaline, and carbonate melts: applications to skarn genesis at Mount Vesuvius. *Geology* 29 (11), 1043–1046. doi:10.1130/0091-7613(2001)029<1043:miroib>2.0.co;2

Iacono-Marziano, G., Gaillard, F., and Pichavant, M. (2008). Limestone assimilation by basaltic magmas: an experimental re-assessment and application to Italian volcanoes. *Contributions Mineralogy Petrology* 155, 719–738. doi:10.1007/s00410-007-0267-8

Iacono-Marziano, G., Gaillard, F., Scaillet, B., Pichavant, M., and Chiodini, G. (2009). Role of non-mantle CO_2 in the dynamics of volcano degassing: the Mount Vesuvius example. *Geology* 37, 319–322. doi:10.1130/g25446a.1

Irvine, T. N., and Baragar, W. R. A. (1971). A guide to the chemical classification of the common volcanic rocks. *Can. J. Earth Sci.* 8, 523–548. doi:10.1139/e71-055

Jolis, E. M., Freda, C., Troll, V. R., Deegan, F. M., Blythe, L. S., McLeod, C. L., et al. (2013). Experimental simulation of magma–carbonate interaction beneath Mt. Vesuvius, Italy. *Vesuvius, Italy. Contrib. Mineral. Petrol.* 166, 1335–1353. doi:10.1007/s00410-013-0931-0

Kang, N., Schmidt, M. W., Poli, S., Connolly, J. A. D., and Franzolin, E. (2016). Melting relations in the system $FeCO_3$–$MgCO_3$ and thermodynamic modelling of Fe–Mg carbonate melts. *Contrib. Mineral. Petrol.* 171, 74. doi:10.1007/s00410-016-1283-3

Kang, N., Schmidt, M. W., Poli, S., Franzolin, E., and Connolly, J. A. D. (2015). Melting of siderite to 20GPa and thermodynamic properties of $FeCO_3$-melt. *Chem. Geol.* 400, 34–43. doi:10.1016/j.chemgeo.2015.02.005

Klebesz, R., Esposito, R., De Vivo, B., and Bodnar, R. J. (2015). Constraints on the origin of sub-effusive nodules from the Sarno (Pomici di Base) eruption of Mt. Somma-Vesuvius (Italy) based on compositions of silicate-melt inclusions and clinopyroxene. *Am. Mineral.* 100, 760–773. doi:10.2138/am-2015-4958

Lima, A., and Esposito, R. (2023). New views on Somma Vesuvius subvolcanic system and on mechanism that could increase eruption explosivity by a review and immiscibility in melt inclusions. *J. Geochem. Explor.* 256, 107348. doi:10.1016/j.gexplo.2023.107348

Lino, L. M., Carvalho, P. R., Vlach, S. R. F., and Quiroz-Valle, F. R. (2023). Evidence for silicate liquid immiscibility in recharging, alkali-rich tholeiitic systems: the role of unmixing in the petrogenesis of intermediate, layered plutonic bodies and bimodal volcanic suites. *Lithos* 450-451, 107193. doi:10.1016/j.lithos.2023.107193

Liu, P., and Jin, Z. (2022). Metamorphic evolution of a tremolite marble from the Dabie UHP Terrane, China: a focus on zircon. *J. Earth Sci.* 33, 493–506. doi:10.1007/s12583-020-1363-1

Lopez-Echeverry, J. S., Reif-Acherman, S., and Araujo-Lopez, E. (2017). Peng-Robinson equation of state: 40 years through cubics. *Fluid Phase Equilibria* 447, 39–71. doi:10.1016/j.fluid.2017.05.007

Martini, M. (1997). "CO_2 emission in volcanic areas: case histories and hazards," in *Plant responses to elevated CO_2*. Editors A. Raschi, F. Miglietta, R. Tognetti, and P. van Gardingen (Cambridge University Press), 34–44.

Mollo, S., Gaeta, M., Freda, C., DiRocco, T., Misiti, V., and Scarlato, P. (2010). Carbonate assimilation in magmas: a reappraisal based on experimental petrology. *Lithos* 114, 503–514. doi:10.1016/j.lithos.2009.10.013

Nikiforov, A. V., Dubinina, E. O., Polyakov, N. A., Sugorakova, A. M., and Khertek, A. K. (2021). Influence of host marble rocks on the formation of intrusive alkaline rocks and carbonatites of Sangilen (E. Siberia, Russia). *Minerals* 11, 666. doi:10.3390/min11070666

Nosova, A. A., Sazonova, L. V., Kargin, A. V., Dubinina, E. O., and Minervina, E. A. (2021). Mineralogy and geochemistry of ocelli in the Damtjernite dykes and sills, Chadobets Uplift, Siberian Craton: evidence of the fluid–lamprophyric magma interaction. *Minerals* 11 (7), 724. doi:10.3390/min11070724

Randive, K., and Meshram, T. (2020). An overview of the carbonatites from the Indian subcontinent. *Open Geosci.* 12, 85–116. doi:10.1515/geo-2020-0007

Remigi, S., Mancini, T., Ferrando, S., and Frezzotti, M. L. (2021). Interlaboratory application of Raman CO_2 densimeter equations: experimental procedure and statistical analysis using bootstrapped confidence intervals. *Appl. Spectrosc.* 75 (7), 867–881. doi:10.1177/0003702820987601

Scheele, N., and Hoefs, J. (1992). Carbon isotope fractionation between calcite, graphite and CO_2: an experimental study. *Contrib. Mineral. Petrol.* 112, 35–45. doi:10.1007/bf00310954

Sharp, Z. D. (1990). A laser-based microanalytical method for the *in situ* determination of oxygen isotope ratios of silicates and oxides. *Geochim. Cosmochim. Acta* 54, 1353–1357. doi:10.1016/0016-7037(90)90160-m

Shvarov, Y. V. (2008). HCh: new potentialities for the thermodynamic simulation of geochemical systems offered by Windows. *Geochem. Int.* 46 (8), 834–839. doi:10.1134/s0016702908080089

Taylor, H. P., Frechen, J., and Degens, E. T. (1967). Oxygen and carbon isotope studies of carbonatites from the Laacher See district, West Germany and the Alno district, Sweden. *Geochim. Cosmochim. Acta* 31, 407–430. doi:10.1016/0016-7037(67)90051-8

Tobin, T. S., Bitz, C. M., and Archer, D. (2017). Modeling climatic effects of carbon dioxide emissions fromDeccan Traps Volcanic Eruptions around the Cretaceous–Paleogene boundary. *Palaeogeogr. Palaeoclimatol. Palaeoecol.* 478, 139–148. doi:10.1016/j.palaeo.2016.05.028

USGS (2004). *NE Asia Geodynamics map, 1:5,000,000*. United States: USGS.

Valley, J. W., Kitchen, N., Kohn, M. J., Niendorf, C. R., and Spicuzza, M. J. (1995). UWG-2, a garnet standard for oxygen isotope ratios: strategies for high precision and accuracy with laser heating. *Geochim. Cosmochim. Acta* 59, 5223–5231. doi:10.1016/0016-7037(95)00386-x

Viladkar, S. G. (2018). Ferrocarbonatites in the amba dongar diatreme, Gujarat, India. *J. Geol. Soc. India* 92, 141–144. doi:10.1007/s12594-018-0972-0

Viladkar, S. G., and Schidlowski, M. (2000). Carbon and oxygen isotope geochemistry of the Amba Dongar carbonatite complex, Gujarat, India. *Gondw. Res.* 3 (3), 415–424. doi:10.1016/s1342-937x(05)70299-9

Wang, X., Chou, I.-M., Hua, W., Burruss, R. C., Sun, Q., and Song, Y. (2011). Raman spectroscopic measurements of CO_2 density: experimental calibration with high-pressure optical cell (HPOC) and fused silica capillary capsule (FSCC) with application to fluid inclusion observations. *Geochim. Cosmochim. Acta* 75, 4080–4093. doi:10.1016/j.gca.2011.04.028

Wojdyr, M. (2010). Fityk: a general-purpose peak fitting program. *J. Appl. Cryst.* 43, 1126–1128. doi:10.1107/s0021889810030499

Xue, Y. X., and Zhu, Y. F. (2007). Genesis of the siderite in jurassic olivine basalt, Karamay, xinjiang, NW China. *Acta Petrol. Sin.* 23 (5), 1108–1122. doi:10.0000/5eb7925da4b74345a065c20f6f711d4a

Zhao, S., Schettino, E., Merlini, M., and Poli, S. (2019). The stability and melting of aragonite: an experimental and thermodynamic model for carbonated eclogites in the mantle. *Lithos* 324-325, 105–114. doi:10.1016/j.lithos.2018.11.005